

(To appear in *Astronomical Journal*, September 1998)

Luminosity Functions and Evolution of Blue Galaxies In A Deep Multicolor CCD Field Survey

Charles T. Liu¹ and Richard F. Green

National Optical Astronomy Observatories, Tucson, AZ 85726

Patrick B. Hall²

Steward Observatory, University of Arizona, Tucson, AZ 85721

and

Patrick S. Osmer

The Ohio State University, Columbus, OH 43210

ABSTRACT

A complete sample of 659 field galaxies with $17.0 < U \leq 21.1$, each with U-B-V-R-I7500-I8600 photometry, has been selected from a deep field survey which covers 0.83 deg^2 along six lines of sight (Hall et al. 1996a). Each galaxy's spectral type and redshift has been estimated using a multicolor photometric technique (Liu & Green 1998). Total number counts of the galaxies in the U-band give a count slope $d(\log N)/dM = 0.55 \pm 0.05$, consistent with previous studies.

The 545 galaxies in the sample classified as spectral type Sbc or bluer are analyzed for signs of evolution with redshift, and for unusual star formation histories. The U-band luminosity function of these blue galaxies at $0.02 < z < 0.15$ has a steep $\alpha \simeq -1.85$ down to $M(B) \simeq -14$. The luminosity functions at $0.15 \leq z < 0.3$ and $0.3 \leq z \leq 0.5$ show significant evolution in M^* and ϕ^* , at levels consistent with those found in the Canada-France and Autofib Redshift Surveys.

A significant population of very blue (rest frame $U-B < -0.35$) galaxies, with spectral energy distributions indicating strong starburst activity, is observed at $z \gtrsim 0.3$ but not at $z < 0.3$. This population is confirmed via spectroscopy of part of the sample. These may be galaxies temporarily brightened by global starbursts, which subsequently fade and redden at lower redshifts.

Subject headings:

¹Current address: Department of Astronomy, Columbia University, 550 E 120 St, New York, NY 10027.

²Currently at the Department of Astronomy, University of Toronto.

1. Introduction

The evolution of field galaxies with redshift is a phenomenon that has been intensely scrutinized, especially recently. It is a subject of debate at every level, including the most basic: what is the zero-redshift galaxy luminosity function? The common approach to this question is to model the luminosity function (LF) using the parameterization of Schechter (1976), which contains a characteristic luminosity M^* , a galaxy space density parameter ϕ^* , and a faint luminosity end with power-law slope α . Thanks to the work of numerous authors on samples of galaxies now totaling upwards of 10^4 objects, a reasonably consistent picture is gradually forming regarding at least two facets of the local LF – with the understanding, of course, that many important details have yet to be reconciled. First, α is probably roughly -1.0 ± 0.3 for the sample of all galaxies in the local universe (see, e.g., Loveday et al. 1992; Marzke et al. 1994a, 1994b; da Costa et al. 1994; Lin et al. 1996). Second, the luminosity functions of blue galaxies, emission-line galaxies and morphologically later-type galaxies tend to have steeper α than redder, non-emitting and earlier-type ones, with estimates ranging from $+0.2$ (Loveday et al. 1992) for early-type galaxies, to -0.9 for galaxies with $[\text{OII}]\lambda 3727 \geq 5\text{\AA}$ (Lin et al. 1996), to -1.87 for morphologically identified Sm-Im galaxies (Marzke et al. 1994b).

As we look at more field galaxy samples with fainter apparent magnitude limits, the key question becomes: how does the luminosity function, and by inference the field galaxy population, evolve with redshift? In the absence of redshift information, faint galaxy counts have been the primary tool for measuring evolution. The case for strong evolution in the field galaxy luminosity function was made, among others, by Maddox et al. (1990), who used number count data – specifically, a steep number count slope $d\log N/dM$ – to show that significant evolution may be occurring in galaxies at $17 < B < 21$. Multicolor surveys such as those of Koo (1986) and Jones et al. (1991) have added dimensions to number count studies by examining the color distributions of galaxies over long wavelength and magnitude baselines. The consensus appears to be that $d\log N/dM$ steepens with decreasing wavelength, suggesting stronger evolution in blue galaxies than red ones. Koo (1986) also used his multicolor data to estimate redshifts in his galaxy population – the so-called photometric redshift technique, which has since been extensively developed – and concluded that an excess of star formation is present in the field galaxy population by $z \sim 0.4$.

Ideally, redshifts for all the galaxies in a survey should be obtained when studying the evolution of those galaxies, because they provide critical information about the distances and absolute magnitudes of each object. Broadhurst, Ellis & Shanks (1988) and Colless et al (1990; 1993) suggested that evolution of the field galaxy luminosity function, probably in the form of increased number density with redshift, was necessary to explain the redshift distribution of their magnitude-limited, $20 \leq B_J \leq 22.5$ survey. Other redshift surveys by Lilly, Cowie & Gardner (1991), Songaila et al. (1994) and Cowie et al. (1996) have concluded that little or no luminosity evolution occurs from $z = 0$ to $z \sim 1$, but suggest the appearance of an additional, starbursting population of objects at high redshift which have since faded – in essence, another sort of number density evolution.

Several recent studies have broken new ground in the study of faint galaxy luminosity functions, by obtaining redshifts for $\sim 10^3$ objects in complete samples of faint galaxies. The Canada-France Redshift Survey (Lilly et al. 1995, hereafter CFRS VI) used an I-band selection criterion to study 730 galaxies with median redshift $\langle z \rangle = 0.56$, and found strong, uniform brightening of the luminosity function among the blue (i.e., with colors of a template Sbc galaxy or bluer) galaxy population. The Autofib Redshift Survey (Ellis et al. 1996; Heyl et al. 1997) assembled over 1700 redshifts from a number of B-band selected samples to study an impressively large magnitude range of $11.5 \lesssim B_J \lesssim 24$. They also found significant evolution of the blue galaxy luminosity function; the faint-end slope of their Schechter function parameterization was a steep $\alpha \sim -1.5$ in their medium and high-redshift bins ($0.15 \leq z \leq 0.35$ and $0.35 \leq z \leq 0.75$, respectively). Most recently, the LF of field galaxies in the CNOC1 Redshift Survey has been analyzed by Lin et al. (1997), who also found that objects with typical Sbc galaxy colors or bluer have a steep $\alpha \simeq -1.4$.

Deep spectroscopic surveys such as these are extremely powerful datasets with which galaxy evolution can be studied in detail. An ideal faint galaxy survey, then, would combine faint limits, large numbers, multicolor photometry and redshifts to look at the evolution of a complete galaxy sample from many directions – luminosity functions, number counts, and spectrophotometric distributions. The primary limiting factor for obtaining such a sample is the enormous amount of telescope time required to measure redshifts with spectroscopy; if reliable redshifts for the survey galaxies could be obtained with colors alone, such a project becomes much more observationally feasible.

In this work, we present the results from a complete U-band selected sample of galaxies from a deep, multicolor CCD survey in six optical and near-infrared passbands. We use a photometric technique to estimate the redshift and spectral type of each galaxy. With those data, we analyze in detail the luminosity function and spectrophotometric properties of the 545 galaxies in the sample with spectral type Sbc or bluer. The multicolor photometry we have measured for each galaxy gives us additional leverage: we minimize possible systematic errors from K-corrections, and we can examine the relative contributions of different-colored galaxies at different redshifts to the observed galaxy population. Our primary goal is to examine the evolution of field galaxies; particularly, we will address the star formation histories of blue field galaxies, to which our U-band selected sample is more sensitive than samples chosen with longer-wavelength passbands. Throughout this paper we use $H_0 = 100h$ km/s/Mpc ($h = 0.8$), and $q_0=0$.

2. Sample Selection and Galaxy Number Counts

Our sample has been assembled from the Deep Multicolor Survey (DMS) of Hall et al. (1996, hereafter HOGPW). The extracted dataset is a complete, magnitude-limited sample of 659 galaxies of all types, with $17.0 \leq U \leq 21.1$. All these galaxies have photometric accuracies of $\sim 10\%$ photometry or better in each of the six DMS passbands U, B, V, R, I75 and I86. The procedures

used for galaxy selection and photometry of the survey galaxies are detailed in Appendix I.

The basic yet informative technique of galaxy number counts is easily applied to our final, complete U-selected dataset, and we do so here. The U-band number counts for all DMS galaxies is shown in Figure 1; the magnitude limit for our sample, $U \leq 21.1$, is marked by the dotted line. We present the plot of the number of galaxies per square degree vs. apparent U magnitude in Figure 2. Also plotted for comparison are number counts from the photographic U-band surveys of Jones et al. (1991), which cover the magnitude range $18 < U < 21$, and Koo (1986), which cover $U > 19$. Those two surveys agree at $U \simeq 21$, but are about a factor of two apart at $U \simeq 19$. (Jones et al. attributed the difference to local large-scale structure.) Our absolute number counts agree very well with Koo (1986), suggesting that the mean field density of the lines of sight covered by the DMS is similar to the SA57 and SA68 fields observed by Koo; that is, we are not likely to be strongly contaminated by clustering at $z \leq 0.5$.

We can compute the slope of the number counts with magnitude, $d \log N / dM$, using an error-weighted least squares fit algorithm; we derive $d \log N / dM = 0.55 \pm 0.05$, an intermediate value between the Jones et al. (1991) and Koo (1986) measurements of 0.49 and 0.68 respectively. These consistency checks give us confidence that our sample is indeed complete and unbiased by significant selection effects or systematic errors.

3. Photometric Measurement of Redshifts and Spectral Types

The application of the photometric techniques developed in Liu & Green (1998, hereafter LG98) to all the galaxies, in order to measure their redshifts and spectral types, is a key step in our analysis of the dataset. We refer the reader to LG98 for a thorough discussion of the method, and present only a brief summary here.

The photometric redshift/typing system we use is grounded on the basic principles first shown by Baum (1962) and later developed further by Koo (1985), Loh & Spillar (1986), Connolly et al. (1995) and others. Essentially, all galaxies not dominated by active galactic nuclei have spectral energy distributions (SEDs) in the near-UV to near-IR wavelength range distinctive enough that, even as they are redshifted into redder observed passbands, their SEDs can be distinguished from galaxies of other types and/or other redshifts with a high level of accuracy with broad-band colors alone, given sufficient wavelength coverage. Although a photometrically determined redshift cannot compare to spectroscopy for measurements of individual galaxies, it can be an excellent statistical tool to examine galaxy populations in large surveys, for which obtaining spectroscopic redshifts is by far the most difficult and expensive in terms of telescope time.

The photometric method of LG98 uses the UBVR_I75I86 data to place galaxies into five spectroscopic categories: E/S0 galaxies (little or no star formation), Sab (weak star formation), Sbc (active star formation), Scd (strongly active star formation), and irregular (starburst). Simultaneously, the method allows us to estimate galaxy redshifts to 1σ accuracies of $\Delta z \sim 0.05$,

and spectral types to within ± 1 galaxy spectral type, in the redshift range $0 < z < 1$. This is essentially the same precision achieved by previous authors with UJFN photographic photometry (e.g., Koo 1985; Connolly et al. 1995) and multicolor photoelectric and CCD photometry (e.g., Loh & Spillar 1986). Since the six-filter dataset slightly “overdetermines” the principal components of most galaxies (Connolly et al. 1995), we can avoid using the apparent magnitude of a galaxy in our redshift determinations. Furthermore, the division of the standard I-band into two narrower bandpasses (I75 and I86) gives us more leverage than the broad I or photographic I_N at higher redshifts, as prominent spectral features such as $H\alpha$ (at $z \sim 0.3$) and the 4000 Å break (at $z \sim 0.9$) are redshifted into that wavelength range. Finally, LG98 uses an algorithm based on empirical data, so incompleteness problems caused by “negative redshift” determinations, which occasionally happen for the Connolly et al. (1995) technique, do not occur.

As discussed in LG98, we emphasize again the difference between the *spectral* type of a galaxy and its *morphological* type. Although there is generally good correspondence between the SED of a galaxy and its position on the Hubble sequence, there are many exceptions to this rule, especially among peculiar galaxies, strongly interacting systems or mergers (see, e.g., Kennicutt 1992; Liu & Kennicutt 1995). In our analysis, we use the derived galaxy spectral types only as a sequence of relative star formation rates and broad-band colors. Except where noted otherwise, we use in this work the terms “spectral type” and “galaxy type” to describe not the morphology of a given galaxy, but rather spectrophotometric properties.

The application of the redshift-type identification algorithm is summarized in Appendix I. Of the 659 galaxies, 104 were classified as E/S0 or Sab galaxies. It has been reasonably well established (see, e.g., Lilly et al. 1995; Ellis et al. 1996; Heyl et al. 1997; Lin et al. 1997) that field ellipticals and early-type spirals evolve little if at all at redshifts less than unity, whereas galaxies with Sbc colors or bluer are the primary contributors to the evolution of the field galaxy population. Since the primary goal of this work is to examine field galaxy evolution, we therefore set aside this subset of early-type galaxies and concentrate our efforts on the rest of the galaxy population — namely, the 545 galaxies in the sample that have been classified as Sbc, Scd or Irr (starburst) galaxies. All subsequent analysis we present in this paper is conducted on the survey galaxies classified as Sbc or bluer, and we refer to them collectively as the blue galaxy sample.

4. Redshift Dependent Luminosity Functions

Constructing the luminosity function of these blue galaxies as a function of redshift is perhaps the best way of quantifying evolution in the blue galaxy population. With our data, an added complication must be taken into account when computing the absolute magnitude of each galaxy: the redshift determined has a large enough error ($\sigma = 0.05$) to affect the luminosity calculation significantly. The method we use to compensate is to treat each galaxy as if it had a probability-weighted distribution in redshift. A similar conceptualization of the problem is discussed in SubbaRao et al. (1996); using the UJFN-derived photometric redshifts of Connolly et

al. (1995) and a modified version of the C-method (Lynden-Bell 1971), they are able to reproduce a spectroscopic-redshift luminosity function rather well. In this work we adopt a modified version of the $1/V_{max}$ formalism (e.g., Schmidt & Green 1986) to compute our redshift-dependent luminosity functions.

4.1. The Probability-Smoothed Luminosity Distribution

Consider a galaxy with an apparent magnitude m_f in a passband f , and redshift $z \pm \sigma$. If $\sigma=0$, then the absolute magnitude is simply

$$M_f = m_f - 5 \log(d_L(z)) - 25.0 - k(z)$$

where $d_L(z)$ is the luminosity distance in megaparsecs, and $k(z)$ is the K-correction in that passband for the spectral energy distribution of the galaxy. The contribution of that galaxy to the luminosity distribution is then a delta function of amplitude unity at redshift z .

In the case where $\sigma > 0$, and the error distribution is Gaussian, the galaxy can be thought of as adding a series of fractional contributions to the luminosity distribution in the redshift space surrounding z . Such a fraction at, for example, redshift $z + \Delta z$ and with a differential redshift width dz , would have an absolute magnitude

$$M'_f = m_f - 5 \log(d_L(z + \Delta z)) - 25.0 - k(z + \Delta z)$$

and have an amplitude

$$N_{z+\Delta z} = P_G(z + \Delta z, z, \sigma) dz / A_G(z + \Delta z, z, \sigma)$$

where P_G and A_G are the Gaussian probability function and its integral, respectively (see, e.g., Bevington & Robinson 1992).

This “fuzzing” of a galaxy’s luminosity distribution in redshift space is straightforwardly achieved numerically, with a choice of $dz \ll \sigma$ to minimize random magnitude errors. For our dataset, $\sigma = 0.05$; our choice of $dz = 10^{-3}$. Our computational algorithm divides each galaxy into a Gaussian-weighted luminosity distribution with 300 bins, from $z-3\sigma$ to $z+3\sigma$ (i.e. $z \pm 0.15$). The entire distribution for each galaxy is normalized to unity.

With the methodology described above, in some cases the luminosity distance is computed with redshifts that are close to zero. As noted by SubbaRao et al. (1996), this can contribute large systematic errors, because near $z = 0$ a small variation in redshift can imply an enormous change in distance modulus and in the accesible volume V_{max} . We therefore consider any fractional luminosity contributions with $z < 0.02$ as sampling the volume within that radius, and make $z = 0.02$ our low redshift cutoff when computing the luminosity function in the low-redshift bin. In any case, galaxies within that volume, corresponding to a recessional velocity $cz < 6000$ km/s, are subject to systematic effects from local large-scale structure and the local supercluster; accounting properly for those effects would be a task in itself, and does not lie within the scope of this work.

Our multicolor survey gives us an additional measure of accuracy when computing the absolute magnitudes of our galaxy. As redshift increases, the accuracy of the magnitude measurement becomes increasingly affected by the inaccuracy of the K-correction – in other words, on the precision with which the SED of the galaxy is actually followed by the SED fitted to it. We can reduce our dependency on this parameter by computing the absolute magnitude of one rest-frame passband using the flux through a observed redder passband for high redshift objects (cf. CFRS VI). As an example, the rest effective wavelength (λ_{eff}) of our U-filter is the same as the observed λ_{eff} of our B-filter at $z = 0.200$. So in the range $0.15 > z > 0.40$, we use the flux through the B-filter, normalized to the rest-frame U-band flux expected for this galaxy, and the appropriate K-correction to the B-filter to compute the absolute U magnitude. In this way, we measure the rest-frame U-band wavelength range much more directly than if we had to rely on a large K-correction.

4.2. The Modified $1/V_{max}$ Method

In the standard $1/V_{max}$ method, each galaxy contributes a weight to the luminosity function equal to the inverse of the accessible volume within which it can be observed. The accessible volume, referred to here as V_{max} , is the total comoving volume within the redshift boundaries of the sample, where the given galaxy could be and fall within the selection criteria of the sample. In our case, the relevant criterion is that its apparent U magnitude lies between 17.0 and 21.1. The available volume is based on the effective solid angle of 0.830 square degree covered by the survey. A disadvantage of the $1/V_{max}$ method for deriving a spatially smoothed luminosity function is that it is sensitive to clustering within the volume; our sample, however, is not likely to be significantly contaminated by clustering, as our number counts above have shown.

In the case of a probability-weighted luminosity distribution for individual objects, it is straightforward to compute V_{max} for each fractional galaxy; correspondingly, its contribution to the luminosity function is $(1/V_{max}) \times N_{z+\Delta z}$. Assembling the luminosity function (LF) is then a matter of summing those contributions within absolute magnitude bins. The error in each magnitude bin was estimated with a standard bootstrap technique, using 200 random samplings (with duplication allowed) of the observed dataset.

4.3. Simulations

The obvious systematic error that comes from creating a luminosity function with “fuzzy” redshifts is that objects near the peak of the distribution will have some part of their light distributed toward brighter magnitudes. Similarly, galaxies toward the bright and faint ends of the absolute magnitude distribution will have some part of their partial contributions scattered into regions which otherwise would have few or no galaxies. This effect will cause us to underestimate

those parts of the LF that contribute the most light, and overestimate those parts which contribute the least. Another systematic error which can arise is that at low redshifts ($z \sim 0.05$), the lower-redshift side of the redshift probability curve contributes significantly more to the luminosity function than the higher-redshift side; this produces a bias toward lower redshifts and luminosities.

To correct for these systematics, we have conducted extensive numerical simulations to quantify the effects of using fuzzy redshifts to derive galaxy luminosity functions. In the ranges $-21 < M^* < -18$, $0.005 < \phi^* < 0.05$ and $-0.8 < \alpha < -2.0$, we created artificial datasets which might be collected by our survey. This was done for each simulated luminosity function by (1) populating a pencil beam survey volume equivalent to the DMS survey with galaxies; (2) “detecting” the galaxies in the volume, given the apparent magnitude limit and known redshift distribution of our survey; (3) adding the redshift uncertainty of our photometric technique ($\sigma_z \simeq 0.05$) to each galaxy; and (4) computing an “observed” LF using our modified $1/V_{max}$ method. For each combination of M^* , ϕ^* and α , we simulated 100 datasets that each detected approximately 545 galaxies with Sbc colors or bluer, and used standard bootstrap methods to estimate the expected spread of resultant luminosity functions.

We illustrate the results of these simulations with two examples. In Figure 3, the dotted line represents the LF of the original parent population of galaxies, while the data points represent the resultant “observed” LF. The parent population was selected from a luminosity function with Schechter parameters $M^* = -19.3$, $\phi^* = 0.0245$, and $\alpha = -1.2$; this is very close to the LF derived from the Autofib Redshift Survey for $0.02 < z < 0.15$ (Ellis et al. 1996). We have computed the resultant “observed” luminosity functions in three redshift bins: $0.02 \leq z < 0.15$, $0.15 \leq z < 0.3$ and $0.3 \leq z \leq 0.5$. The systematic effects are clearly evident, and differential with redshift as well; the low-redshift LF appears to have a steeper faint-end slope, while the medium- and high-redshift LFs seem to have much higher M^* . For all three LFs, ϕ^* is observed to be lower than the parent population’s original value.

The results of a similar set of simulations, but with $\alpha = -1.8$, are presented in Figure 4. This time, although the M^* and ϕ^* effects are qualitatively similar to those in Figure 3, the “observed” results reflect α much more accurately in the low-redshift bin. (In the medium- and high-redshift bins, not enough faint galaxies are observed to make an accurate measurement of α ; this is consistent with the actual survey data as well.) The reduced distortion in α with increasingly steep LFs is consistent with the analysis of fuzzy redshift LFs in SubbaRao et al. (1996).

Our simulations show that the numerical effects of the fuzzy redshift, although sometimes severe, are predictable and repeatable. This means that the luminosity functions in each redshift bin can be properly and unambiguously corrected to reflect more accurately the original parent luminosity function. The amount of correction needed varies depending on the parameters of the parent LF, and the M^* and ϕ^* determined after corrections are applied are still uncertain at about the 25% level. However, the faint-end slope of the luminosity function is very accurately reproduced ($\Delta\alpha = \pm 0.05$) as long as the data extend to at least $M \simeq -16$.

Using the corrections computed with our simulations, we correct the LF measurements in each magnitude bin, within each redshift bin. We then compute the U-band luminosity functions for our blue galaxy sample in the three redshift bins mentioned above: low- ($0.02 \leq z < 0.15$), medium- ($0.15 \leq z < 0.30$), and high-redshift ($0.30 \leq z \leq 0.50$). These bins correspond approximately with the redshift bins adopted by other authors for ease of comparison. Coincidentally, they also suit the Sbc-and-bluer galaxy sample very naturally; there are similar numbers of objects within each bin (161, 181 and 195 galaxies respectively), and there are only 8 objects in the sample with $z > 0.5$.

4.4. The U-band Luminosity Function vs. Redshift

We present the corrected U-band luminosity functions for the blue galaxy sample in Figure 5. The 1σ error contours for the low-redshift LF are presented in Figure 6.

Using the standard Schechter (1976) parameterization, the faint end slope of the low-redshift LF is best fit with a power law $\alpha = -1.85 \pm 0.15$. This slope is very steep compared to the derived Schechter-parameterized α 's of $\sim 0.9 \pm 0.1$ found in the local blue galaxy luminosity function measurements of Lin et al. (1996), Marzke et al. (1994), Loveday et al. (1992) and others; it is also steeper than the values of $\alpha = 1.25$ to 1.44 measured by Ellis et al. (1996) and Heyl et al. (1997) for various emission-line and blue galaxy subsets in the Autofib redshift survey.

Interestingly, we note that Marzke et al. (1994) measured the luminosity function for morphologically selected Sm-Im galaxies in the CfA Redshift Survey, and derived a value of $\alpha = -1.87$. The fact that the U-band LF faint-end slope is so similar to that of local Magellanic spirals and irregulars suggests that we are seeing objects with spectrophotometric properties typical of Magellanic galaxies – that is, blue and actively forming stars.

Aside from color selection, we may also be selecting more low-surface brightness galaxies than a typical one or two-passband sample; by using any three of six passbands to identify a galaxy, selecting an aperture size with a redder passband, and then measuring all the U-band flux in that relatively large aperture, we may be allowing more objects with low U-band surface brightness into the sample. (Our central surface brightness limit is $\mu_o(U) = 22.6$ magnitudes per square arcsecond.) Since low-luminosity, low-surface brightness galaxies tend to be bluer and may be quite numerous (De Jong 1995; McGaugh, Bothun & Schombert 1995), and Magellanic galaxies tend also to have lower surface brightness, the similarly steep slope of our LF and the Marzke et al. (1994) Sm-Im LF may be due in part to a less severe surface brightness selection effect in these samples compared to other samples used to compute LFs.

We note also that the surveys of faint galaxies in clusters at $z \sim 0.2$ conducted by Smith, Driver & Phillips (1997) and Wilson et al. (1997) have found steep α 's of -1.7 to -2 in those galaxy populations as well. Wilson et al. further suggest that many of the fainter galaxies in their sample may have faded significantly in surface brightness since $z = 0.2$; and Smith et al. speculate

that such steep faint-end slopes may hold for field galaxies as well (see also Driver & Phillips 1996). It is an intriguing possibility that the U-selected, blue field galaxy LF is drawn from the same population as faint galaxies in rich clusters; their very similar faint-end slopes lend some credence to this hypothesis.

4.5. The U-band Luminosity Function From $z = 0.15$ to 0.50

In our medium-redshift and high-redshift bins, the U-band apparent magnitude limit allows us to sample only relatively bright galaxies ($M(U) \sim -18$ or brighter). Schechter function fits to these bright-end segments of the LFs, therefore, do not constrain α very rigorously. We can, however, measure the relative changes in M^* and ϕ^* by fixing the LF segments to α 's consistent with the respective redshift bins, and finding the best fit to the other two parameters.

The fits to the data were all obtained using an error-weighted least squares algorithm. Good fits were possible for both segments in the range $-1.4 \leq \alpha \leq -1.8$; so we adopted the value in the center of that range, $\alpha = -1.6$. Next, the best fit for the medium-redshift bin, with M^* and ϕ^* as free parameters, was computed with fixed α . (We emphasize once more that these values are not meant to be “measurements” of these parameters. Our intent is to use them as benchmarks, to quantify our comparison of the medium and high-redshift LFs.) Finally, we started from these values and moved M^* and ϕ^* until a good fit to the data was achieved with the high-redshift LF segment. The faintest luminosity bin in the high-redshift LF segment is affected by incompleteness, and we do not include it in the fit. Since the high-redshift segments barely reach M^* , ϕ^* can easily be varied as much as a factor of 50% or more (with a smaller corresponding move of M^*) and excellent fits can still be achieved; we thus chose the smallest possible change in ϕ^* that produced a good fit to the data. In this way, we can give a lower bound to the number density evolution we might expect as the average redshift of our sample increases from $\langle z \rangle \sim 0.2$ to $\langle z \rangle \sim 0.4$.

The best-fit Schechter function fit for the medium-redshift bin was $M^* = -19.61$ and $\phi^* = 0.0147$. With the prescription described above, the high-redshift bin was best fit with $M^* = -19.85$ and $\phi^* = 0.0187$. In other words, ϕ^* increases 30% and M^* brightens by 0.25 magnitude. The formal errors to these fits are relatively large – ~ 0.2 magnitude in M^* , $\sim 25\%$ in ϕ^* – but the trend is clear, even upon visual inspection of Figure 5. Our fitting procedure, which attempts to produce the smallest possible shift in ϕ^* , also supports the idea that we are seeing real evolution in the galaxy population.

Comparison with the CFRS and Autofib data shows that our results are consistent with the evolution observed in those surveys. In CFRS VI, M^* in their blue galaxy luminosity functions brightens by about 1 magnitude, assuming no change in ϕ^* , between their redshift bins $0.2 < z < 0.5$ and $0.5 < z < 0.75$. Our brightening of 0.25 magnitude occurs largely within their low-redshift bin; it can be increased to ~ 0.5 magnitude if we fit the parts of our LF that correspond to the same magnitude ranges observed in the CFRS and hold ϕ^* fixed. Both these values are consistent

with an incremental brightening of M^* from $\langle z \rangle \sim 0.2$ to $\langle z \rangle \sim 0.4$, which leads to a total brightening of ~ 1 magnitude by $\langle z \rangle \sim 0.6-0.7$. Heyl et al. (1997) parameterized the Autofib data with redshift-dependent evolving luminosity functions as a function of galaxy spectral type (determined by cross-correlation of spectral features with galaxy templates); based on those models, we can estimate the expected evolution in the combined population of Sbc, Scd and Sdm/starburst spectral types from $\langle z \rangle \sim 0.2$ to $\langle z \rangle \sim 0.4$. For that interval, M^* would brighten by ~ 0.1 magnitude and ϕ^* would increase $\sim 50\%$. This solution is also allowed by our fits, which as we mentioned above can easily accommodate an increase in ϕ^* by reducing ΔM^* .

5. An Excess Starbursting Population At $z > 0.3$

All of our measurements of the evolution of the blue galaxy LF with redshift are consistent with those observed by other workers using deeper surveys. We can now use the added dimension of multicolor observations in our survey to examine the spectrophotometric properties of the galaxies themselves, and see which kinds of galaxies are contributing most to the evolution.

We can glance at the distribution of color vs. magnitude for the entire blue galaxy sample in Figure 7. We plot rest frame (U-B) vs. absolute U magnitude, with different symbols representing the different redshift bins. The majority of the sample objects lie around (U-B) ~ -0.1 , as expected for a population dominated by late-type spirals and starburst galaxies. The reddest galaxies in the sample have (U-B) ~ 0.2 ; this is determined by our blue galaxy selection criterion. As (U-B) decreases, a progressively stronger young stellar population dominates the luminosity, implying increasingly active star formation. A dotted line at (U-B) = -0.35 is provided in the figure, to mark the approximate color of a galaxy with an ongoing global starburst.

Below this line at (U-B) = -0.35 , objects from the high-redshift bin outnumber objects from the lower-redshift bins by a factor of two. At first glance this may not seem surprising, since the high-redshift bin samples a comoving volume about twice that of the two lower redshift bins combined. The respective fractions of these objects in their bins, however, is significantly different: less than 4% for the lower redshift bins, compared to 10% at high redshift. The difference cannot be attributed to random errors alone.

A quantitative display of this effect is shown in Figure 8. The galaxies have been placed into nine bins – 3 U-band luminosity bins, in each of the three redshift bins – and plotted in histogram form. (Bins containing no galaxies are plotted for reference.) In the vertical direction, going down, the galaxies in the same redshift bin increase in luminosity. Down each column, in each redshift, we see the well known color-magnitude relation, where brighter galaxies tend to have redder colors. But across the rows, the magnitude bins remain constant, and only redshift changes; although the number of galaxies in each bin varies widely, the color evolution with redshift is evident. For example, the median (U-B) color of the high-redshift bin from $-19.1 < M(U) < -21.1$ is about 0.1 magnitude bluer than those at medium-redshift, and about 0.2 magnitude bluer than those at

low-redshift. The trend exists regardless of what boundaries for the luminosity bins are chosen.

We test the possibility that this is a magnitude-limited selection effect by plotting the same figure with a brighter limiting magnitude of $U \leq 20.8$ instead of $U \leq 21.1$, and present it in Figure 9. The number of galaxies is reduced, so the statistics are less reliable. Nonetheless, the same effect is observed, and the median colors for each bin are essentially unchanged.

As a further check on the excess of very blue galaxies in the high-redshift bin, we examine the U, B, and R images of these galaxies in the survey data. Each galaxy appears to have an atypically bright U-band image, with no signs of undiscovered cosmic rays, uncorrected bad pixels, or other problems in the data that would have artificially caused the colors to be so blue. If they existed at low redshift, these objects would easily have been detected — and even preferentially selected — in our U-selected survey. But there are almost no such galaxies in bins (d) and (g) of Figures 8 and 9. The implication seems to be that a significant population of very blue, probably starbursting galaxies appears at $z \gtrsim 0.3$ which are not observed at $z < 0.3$.

5.1. Spectroscopic Confirmation

There remains the possibility that these very blue objects are not actually galaxies at the redshifts we believe, but rather artifacts caused by incorrectly determined photometric redshifts. We thus use spectroscopy to confirm that this excess starbursting population exists.

Spectra were obtained using the the Boller & Chivens Spectrograph on the Steward Observatory 2.3-meter telescope at Kitt Peak on December 1996 and January 1997. We used a $4''.5 \times 180''$ longslit and a 400 l/mm grating, to obtain spectra from 3650 Å to 7000 Å. By using the large slit width, we were able to obtain essentially integrated spectra of the objects and avoid problems with differential atmospheric refraction. Spectral resolution was usually not limited by the slit width, and was typically ~ 15 Å. We also observed spectrophotometric standard stars to obtain relative spectrophotometry for the galaxies. Standard data reduction techniques using the IRAF software system were used to process the longslit data, primarily with the CCDRED and LONGSLIT packages. Apertures along the slit were traced and extracted with the APEXTRACT package.

The apparent magnitudes and integration times of the objects we observed are given in Table 1. Usually, it is rather difficult to obtain spectra for 20th magnitude or fainter objects with a 2-meter class telescope; but the high sensitivity of the Steward 800x1200 CCD, combined with the strong emission lines of the targets, allowed us to obtain unambiguous redshifts for all 9 blue objects we observed. The color redshift determinations and spectroscopic measurements are also given in Table 1. The mean absolute deviation of the photometric vs. spectroscopic redshifts is $\Delta z = 0.043$, exactly consistent with the accuracy level we predict for our redshift estimation algorithm (LG98).

Four of the spectra are shown in Figure 10. We overplot the redshifted spectral energy distribution of our starburst template over each spectrum (*dotted line*) for comparison; the continua for both the templates and the galaxies have been normalized to unity at the $[\text{OII}]\lambda 3727$ Å emission line. The spectra show that these galaxies are indeed blue galaxies similar to the template starburst galaxy. This further confirms that our observed excess starburst population is real.

6. Discussion

The idea of a bursting population at relatively high redshift that has since faded has been put forth, among others, by Broadhurst, Ellis & Shanks (1988), Lacey & Silk (1991), Babul & Rees (1992), and Cowie et al. (1996). The application of those models, however, is primarily to the so-called “faint blue galaxies,” (see, e.g., Ellis 1997) where galaxy counts beyond $B \sim 22$ are much greater than expected for a non-evolving population. Our blue galaxy survey from the DMS only reaches $B \sim 21$; thus it is probably inappropriate to call the excess starburst galaxies in our high-redshift bin “faint blue galaxies” in the above sense. However, our data certainly suggest that our starbursts may be related to that faint blue galaxy population, and in fact may be the lowest redshift examples of those distant and numerous blue objects.

What these $z \gtrsim 0.3$ high redshift starburst galaxies may help explain is the general evolution of the blue galaxy luminosity function. We have confirmed the results of Koo (1986), CFRS VI, Ellis et al. (1996), Heyl et al. (1997), Lin et al. (1997) and others that evolution does occur in the blue field galaxy population, and that the evolution is observationally discernible by $z \simeq 0.3$. The number density and/or luminosity increases we are seeing may in fact be caused in part by the appearance of these starbursting objects. No galaxy can long sustain the gas consumption rate required to produce the strong global star formation implied by their (U–R) and (U–B) colors; so these objects should eventually fade, then redden, and eventually blend into the more numerous population of galaxies with lower, steady-state star formation.

Can such starburst galaxies fade into the background of more quiescent galaxies in the time between our high-redshift and medium-redshift bins? We examine this question using the population synthesis models of Bruzual & Charlot (1993), which give us quantitative estimates of the colors and magnitudes of aging starbursts. We first consider the most extreme case, of a galaxy starbursting so strongly that its underlying stellar population contributes negligibly to the total luminosity of the galaxy. For this case, we use an instantaneous burst model with a Salpeter initial mass function. In our chosen cosmology, 1.4×10^9 years elapse between $z=0.4$ and $z=0.2$, roughly the mean redshift of the galaxies in our high-redshift and low-redshift bins respectively. We assume that we are observing the burst at an age where the rest frame (U–B) and (U–R) colors most closely match those of the starburst galaxies in the high-redshift bin. That age would be 6×10^7 years, when (U–B) = -0.49 and (U–R) = 0.28 . After 1.4×10^9 yr the U magnitude of the burst will have faded over 4 magnitudes according to the Bruzual & Charlot models, and

the colors will have reddened to $(U-B) = 0.24$ and $(U-R) = 1.3$. If $M(U) \sim -21$ at 6×10^7 yr, the post-burst evolution moves the galaxy well into the middle of the locus where most of the low-redshift galaxies lie in Figure 7. Our survey would not be able to detect such an object at $z \sim 0.2$.

A somewhat less extreme case would be a galaxy which has a global starburst triggered in it. In one possible scenario, explored by Charlot & Silk (1994), Belloni et al. (1995), Barger et al. (1996) and others, the starburst continues at a constant star formation rate for a short time (typically 10^8 to 10^9 yr), then stops after converting into stars a gas fraction equal to some percentage (typically 10-20%) of the final mass of the galaxy. After this burst is over, all star formation is truncated. We choose for our comparison a late-type spiral galaxy which undergoes a Salpeter-IMF starburst lasting 10^8 yr that consumes 10% of the final galaxy mass. If we select a time after the starburst begins when the galaxy has UBR colors similar to our template starburst, these authors show that $(U-B)$ will again be $\gtrsim 0.2$ after 1.4 Gyr; the U-band fading would be a more modest ~ 2 magnitudes. This burst scenario would move our $M(U) \sim -21$ bursting galaxy into the middle of the medium-redshift galaxy locus, again becoming largely anonymous within a large reservoir of ordinarily-colored blue galaxies.

If fading and reddening of the burst is indeed the mechanism for removing starburst galaxies from view nearward of $z \sim 0.3$, one strong test of this population's effect on the blue galaxy luminosity function would be to see if removing the excess starburst galaxies leads to a luminosity function consistent with a passively evolving galaxy population since $\langle z \rangle \sim 0.4$. Our photometry is unfortunately not deep enough to let us conduct this test rigorously. A firm conclusion can be drawn when additional data for galaxies at fainter absolute magnitudes become available.

7. Conclusions

We have shown that an optical multicolor survey of field galaxies, such as the Deep Multicolor Survey, can be a very powerful tool for studying galaxy evolution. Such a survey offers concrete advantages over surveys with only one or two passbands: the two most relevant in this work are our decreased dependence on K-corrections for accurate absolute magnitude determinations, and the additional leverage we obtain from examining the spectral energy distributions of each galaxy. In addition, while there is ultimately no substitute for secure spectroscopic redshifts, we can extract almost as much information about luminosity functions and evolution as a function of redshift as true redshift surveys by using a photometric redshift-classification technique such as we have, with orders of magnitude less telescope time. We have developed a modified version of the $1/V_{max}$ method for computing luminosity functions using galaxies with photometrically determined redshifts. The method's systematic errors make absolute determinations of M^* and ϕ^* difficult; but relative changes in the luminosity functions are reliably measured, and can be effectively used to study differential evolution.

We have assembled a complete, magnitude limited sample of 545 galaxies with rest-frame multicolors as blue as, or bluer than, a typical Sbc galaxy. The low-redshift ($0.02 \leq z < 0.15$) luminosity function for this sample has a very steep faint-end slope, which turns out to be consistent with the measurement of α for Magellanic spirals and irregulars from the CfA Redshift Survey (Marzke et al. 1994). The implication is that our blue galaxies and those Sm-Im galaxies are drawn from essentially the same steep-sloped population. Whether that population is defined by its spectrophotometric, morphological or surface-brightness properties is uncertain, and merits further investigation.

U-band number counts vs. redshift, and comparison of the luminosity function segments in medium-redshift ($0.15 \leq z < 0.30$) and high-redshift ($0.30 \leq z \leq 0.50$) bins, demonstrate significant evolution in the galaxy population which is clearly visible by $z \gtrsim 0.3$. The nature, amplitude and epoch of the evolution we observe are consistent with those found by the Canada-France Redshift Survey and the Autofib redshift survey. Using the broad wavelength coverage for each galaxy in our survey, we use color-magnitude diagrams and histograms in (U–B) vs. absolute magnitude to identify an excess population of apparently starbursting galaxies in the high-redshift bin which does not appear at lower redshift. It is plausible that these objects have been temporarily brightened by their global starbursts, and will redden and fade into obscurity by $z \sim 0.2$. These galaxies may be contributing significantly to the observed evolution of the blue galaxy luminosity function at $z \gtrsim 0.3$. If this is true, what makes the particular epoch $z \simeq 0.3$ the threshold past which these starbursts are no longer produced? The answer to that question will contribute greatly to our understanding of field galaxy evolution.

We thank Rob Kennicutt, Jim Liebert, Hans-Walter Rix and Jon Gardner for helpful discussions. We thank the referee for a detailed and very constructive critique which has significantly improved this work.

A. Appendix I

The Deep Multicolor Survey: Galaxy Detection, Photometry, and Redshift-Type Identification

A detailed description of the Deep Multicolor Survey (DMS) is given in HOGPW. Here, we summarize its characteristics, and describe how the galaxy sample is derived.

The DMS was obtained with the Mayall 4-meter telescope at KPNO, in direct imaging mode at prime focus, with an engineering quality 2048×2048 Tektronix CCD. The survey covers 0.83 deg^2 along six lines of sight at high galactic latitude. Each field was observed with six filters: standard Johnson UBV; a custom R filter calibrated to the Kron-Cousins system; and two custom I filters with $\lambda_{eff} = 7430 \text{ \AA}$ and 8520 \AA respectively, referred to hereafter as I75 and I86. Reduction and calibration of the images, and the establishment of the photometric system for the

nonstandard filters, was performed as described in HOGPW.

The assembly of the object catalog was performed in several steps. First, the Faint Object Classification and Analysis System (FOCAS; Valdes 1982a) was used to identify objects using its default (“built-in”) detection filter. The detected objects were classified using the “resolution” task in FOCAS (Valdes 1982b) as star, fuzzy star, galaxy, diffuse object, or noise, using templates generated from a point source function empirically determined from the CCD image. An inclusive, automatically generated galaxy catalog was then assembled using all the objects classified as galaxies in at least three filters. In all but one of the surveyed lines of sight, two exposures were taken in each passband; in those cases, “resolution” had to classify an object as a galaxy in both exposures for it to be declared a galaxy in that passband. This inclusive catalog contained 9,431 objects.

The second step was to use the IRAF package APPHOT to obtain aperture photometry of each object in the catalog described above. Each galaxy’s flux was measured with concentric circular apertures ranging from 10 to 30 pixels ($5''.3$ to $15''.9$) in diameter. Instrumental magnitudes and Poisson signal-to-noise were measured for each aperture; the sky value was computed separately for each object by taking the mode of the pixel values in an annulus around the aperture center, typically with inner diameter 32 pixels ($17''.0$) and outer diameter 50 pixels ($26''.5$).

An aperture optimization technique, similar to the growth curve optimization method used by Yee, Green & Stockman (1986), was then applied to each object. The function of the object’s Poisson signal-to-noise vs. aperture radius was examined and the optimal size was determined to be either: (1) at the 30 pixel diameter ($15''.9$) limit; or (2) where the next largest aperture showed an inflection point, indicating an intruding object or cosmic ray, or a decrease much larger than expected from the addition of random sky noise. The aperture size selection was performed using the R-band data, the passband with the greatest depth, for each object; extinction and color-corrected magnitudes were then extracted with the same aperture size in all six passbands.

The U-band magnitude selection limit for our blue galaxy sample was determined by our desire to have a complete sample with good signal-to-noise in all passbands for each galaxy. In the DMS, this meant a typical magnitude of $U \lesssim 21.1$ for a galaxy with surface brightness levels typical of a Magellanic spiral. Visual inspection of the raw number counts, presented in Figure 1, shows that this is over a magnitude brighter than the U-band completeness limit of $U_{lim} \sim 22.2$; thus we are confident that such a selection limit would also be a complete, magnitude-limited sample.

To make sure all the galaxies within our magnitude limit would be included, we took the subset of all the objects in the inclusive survey brighter than $U=21.2$ – the magnitude limit desired, plus the typical 1σ photometric error at that limit – and inspected them visually. Using the IMEXAM task in IRAF, we checked that the automatically optimized aperture for each galaxy was indeed appropriate – that is, inclusive of all the galaxy light within the sky-limited isophotal

magnitude, and not inclusive of nearby objects. Objects with stars or very large (>6 contiguous pixels) cosmic rays within the radius of our minimum aperture size ($2''.6$) were removed from the sample; these objects comprised about 5% (44 out of 953) of the original subsample. In cases where the aperture optimization algorithm was “deceived” (e.g., by a highly edge-on galaxy, or a strongly interacting system), the aperture size was adjusted appropriately.

The instrumental fluxes for the visually adjusted apertures were then extracted from the photometry database. Smaller, visually obvious cosmic rays in or near the apertures that were not removed in the initial calibration and reduction of the image frames (see HOGPW) were removed by hand using the FIXPIX task in IRAF, which replaces the affected pixels with a value interpolated from the surrounding pixels. Extinction and color-corrected magnitudes were again computed. In the lines of sight where two frames were available for each passband, a final additional check was made for cosmic rays and bad pixels: if the signal-to-noise of one image in a given filter was more than 150% of the other image, it was assumed that a cosmic ray, chip defect or other systematic error was contaminating that image, and the uninflated measurement was used. Otherwise, the final magnitude for each bandpass was computed as a signal-to-noise weighted average of the two measurements. All the objects with $17.0 \leq U \leq 21.1$ were then extracted. This subsample contains 667 objects.

Finally, every object in the sample was processed using the “GetZ” program as described in LG98. “GetZ” implements the photometric redshift-spectral classification algorithm (see Section 3), and outputs a redshift and a spectral type (E/S0, Sab, Sbc, Scd, or Irr). “GetZ” did not find an acceptable solution to 8 objects; inspection showed that all of these objects appeared to be point sources or nearly so. These objects were taken to be misclassified stars, and removed from the sample. There is a small possibility that these objects were AGN, whose colors are sufficiently different from the template galaxies that “GetZ” could not find redshift-type matches. Their removal in any case should not affect our conclusions, since their numerical contribution to the total sample is so small (barely 1%). The final sample contains 659 galaxies, each of which has $\sim 10\%$ or better photometry in all six passbands.

Table 1. Spectroscopic Results

Galaxy ID	mag(B)	Exposure	z_{phot}	z_{spec}
01a-521-225	20.75	2300s	0.250	0.239
01a-1085-740	20.54	2500s	0.250	0.245
01a-632-1866	21.27	3600s	0.275	0.236
10a-1762-311	20.07	3600s	0.300	0.109
01a-246-1506	20.56	4800s	0.325	0.283
10a-636-1395	21.41	2400s	0.325	0.296
01a-1680-382	21.50	4000s	0.375	0.360
01a-448-224	20.84	2300s	0.400	0.430
01a-1029-680	20.94	3600s	0.475	0.492

REFERENCES

- Babul, A., & Rees, M. J. 1992, MNRAS, 255, 346.
- Barger, A., Aragón-Salamanca, A., Ellis, R., Couch, W., Smail, I., & Sharples, R. 1996, MNRAS, 279, 1.
- Baum, W. A. 1962, Problems of Extragalactic Research, IAU Symposium No. 15 (MacMillan, New York), 390.
- Belloni, P., Bruzual, G., Thimm, G., & Roeser, H.-J. 1995, A&A, in press.
- Bevington, P. R., & Robinson, D. K. 1992, Data Reduction and Error Analysis For The Physical Sciences, New York: McGraw-Hill.
- Broadhurst, T., Ellis, R. S., & Shanks, T. 1988, MNRAS, 235, 827.
- Bruzual A., G., & Charlot, S. 1993, ApJ, 405, 538.
- Charlot, S., & Silk, J. 1994, ApJ, 432, 453.
- Colless, M., Ellis, R. S., Broadhurst, T., Taylor, K., & Peterson, B 1993, MNRAS, 261, 19.
- Colless, M., Ellis, R. S., Taylor, K., & Hook, R. N. 1990, MNRAS, 244, 408.
- Connolly, A. J., Csabai, I., Szalay, A. S., Koo, D. C., Kron, R. C., & Munn, J. A. 1995, AJ, 110, 2655.
- da Costa, L. N., et al. 1994, ApJ, 424, L1.
- Cowie, L. L., Songaila, A., Hu, E., & Cohen, J. 1996, AJ, 112, 839.
- Driver, S. P., & Phillipps, S. 1996, ApJ, 469, 529.
- Ellis, R. S. 1997, ARA&A, 35, 389.
- Ellis, R. S., Colless, M., Broadhurst, T., Heyl, J., & Glazebrook, K. 1996, MNRAS, 280, 235.
- Green, R. F., & Schmidt, M. 1978, ApJ, 220, L1.
- Hall, P. B., Osmer, P. S., Green, R. F., Porter, A. C., & Warren, S. J. 1996 (HOGPW), ApJS, 104, 185.
- Hammer, F., Flores, H., Lilly, S. J., Crampton, D., Le Fèvre, O., Rola, C., Mallen-Ornelas, G., Schade, D., & Tresse, L. 1997, ApJ, 481, 49.
- Heyl, J., Colless, M., Ellis, R. S., & Broadhurst, T. 1997, MNRAS, 285, 613.
- Jones, L. R., Fong, R., Shanks, T., Ellis, R. S., & Peterson, B. A. 1991, MNRAS, 249, 481.
- de Jong, R. S. 1995, Ph. D. Thesis, University of Groningen.
- Kennicutt, R. C. 1992, ApJS, 79, 255.
- Koo, D. C. 1985, AJ, 90, 418.
- Koo, D. C. 1986, ApJ, 311, 651.

- Lilly, S. J., Tresse, L., Hammer, F., Crampton, D., & Le Fèvre, O. 1995 (CFRS VI), *ApJ*, 455, 108.
- Lilly, S., J., Cowie, L. L., & Gardner, J. P. 1991, *ApJ*, 369, 79.
- Lin, H., Kirschner, R., Schectman, S., Landy, S., Oemler, A., Tucker, D., & Schechter, P. L. 1996, *ApJ*, 464, 60.
- Lin, H., Yee, H. K. C., Carlberg, R. G. & Ellingson, E. 1997, *ApJ*, 475, 494.
- Liu, C. T., & Green, R. F. 1996 (LG98), *AJ*, submitted.
- Liu, C. T., & Kennicutt, R. C. 1995, *ApJS*, 100, 325.
- Loh, E. D., & Spillar, E. J. 1986, *ApJ*, 303, 154.
- Loveday, J., Peterson, B. A., Efstathiou, G., & Maddox, S. J. 1992, *ApJ*, 390, 338.
- Lynden-Bell, D. 1971, *MNRAS*, 155, 95.
- Maddox, S. J., Sutherland, W. J., Efstathiou, G., Loveday, J., & Peterson, B. A. 1990, *MNRAS*, 247, 1P.
- Marzke, R. O., Geller, M. J., Huchra, J. P., & Corwin, H. 1994, *AJ*, 108, 437.
- McGaugh, S., Bothun, G., & Schombert, J. 1995, *AJ*, 110, 573.
- Schechter, P. 1976, *ApJ*, 203, 297.
- Schmidt, M., & Green, R. F. 1986, *ApJ*, 305, 68.
- Smith, R. M., Driver, S. P., & Phillipps, S. 1997, *MNRAS*, 287, 415.
- Songaila, A., Cowie, L. L., Hu, E. M., & Gardner, J. P. 1994, *ApJS*, 94, 461.
- SubbaRao, M. U., Connolly, A. J., Szalay, A. S., & Koo, D. C. 1996, *AJ*, 112, 929.
- Valdes, F. 1982a, *FOCAS User's Manual*, (Tucson: Kitt Peak National Observatory, Central Computer Services)
- Valdes, F. 1982b, in *Instrumentation in Astronomy IV*, ed. D. L. Crawford (*Proc. SPIE*, Vol. 331), 1982.
- Wilson, G., Smail, I., Ellis, R. S., & Couch, W. J. 1997, *MNRAS*, 284, 915.
- Yee, H. K. C., Green, R.F., & Stockman, H. S. 1986, *ApJS*, 62, 681.

Fig. 1 Total raw U-band galaxy number counts for the Deep Multicolor Survey. The dotted line at $U=21.1$ denotes the magnitude limit for the U-selected sample.

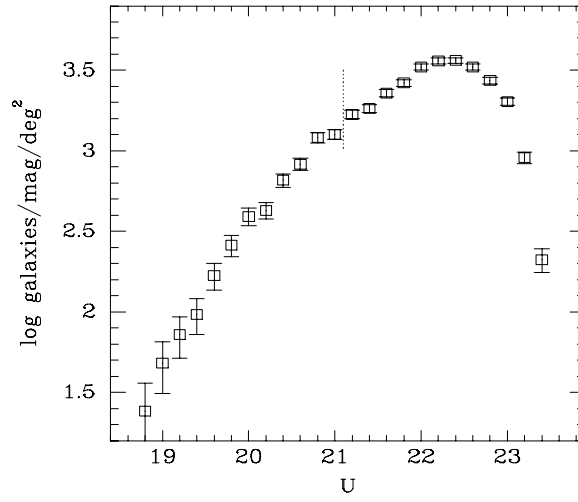


Fig. 2 U-band number counts in the U-selected sample (dark circles). Also plotted are the photographic U-band number counts of Koo (1986) and Jones et al. (1991).

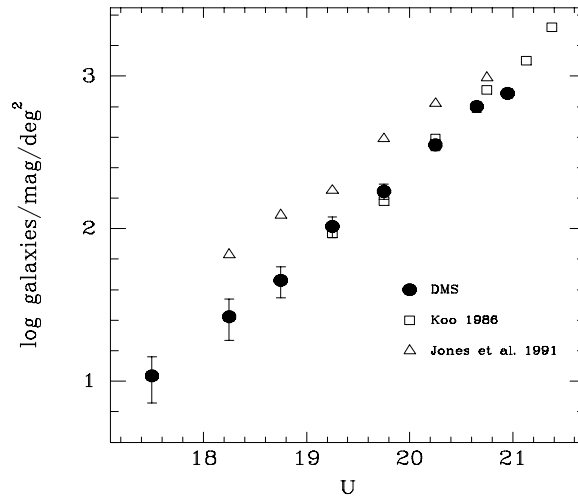


Fig. 3 Results of simulated observations using fuzzy redshifts. *Solid line*: model luminosity function with $M^* = -19.3$, $\phi_* = 0.0245$ and $\alpha = -1.2$. The points are the luminosity functions recovered by the simulated observations for low, medium and high redshift bins.

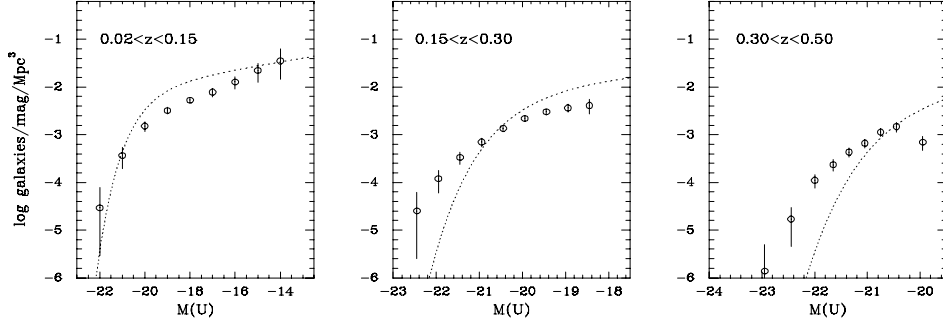


Fig. 4 Same as Fig. 3, but with $\alpha = -1.8$.

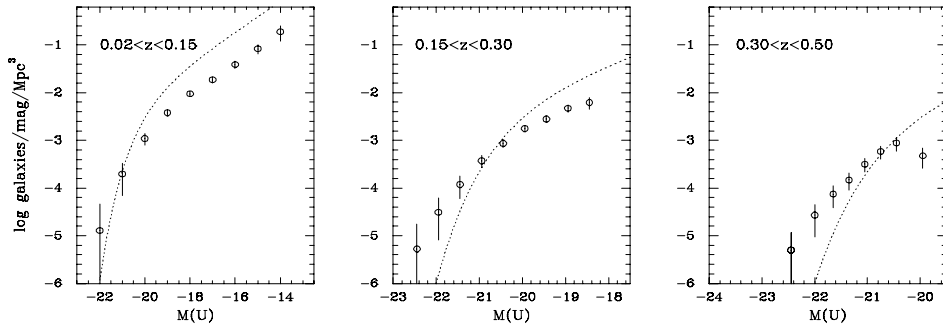


Fig. 5 Luminosity functions constructed from the probability-weighted luminosity distributions of the blue (Sbc and bluer) galaxy sample.

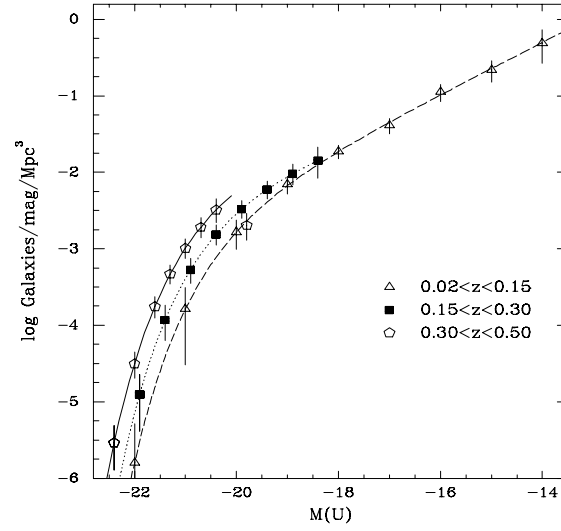


Fig. 6 1σ error contours for Schechter function fit parameters for the low-redshift ($0.02 < z < 0.15$) luminosity function of the blue galaxy sample. The point in the center of each contour marks the Schechter function fit presented in Figure 3.

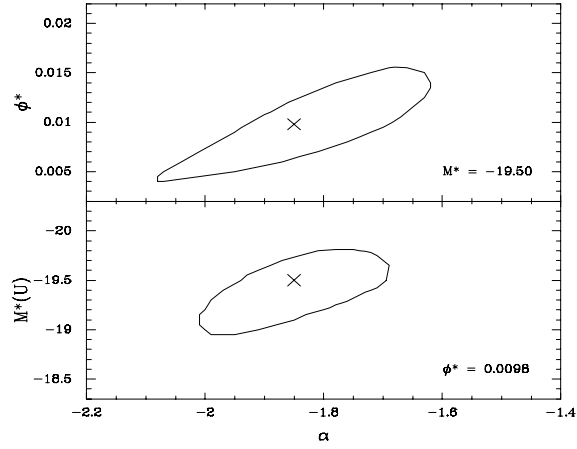


Fig. 7 Absolute R magnitude vs. rest frame (U-B) color for the blue galaxy sample. The symbol for each galaxy denotes its location in the low (triangles), medium (squares) or high (circles) redshift bin.

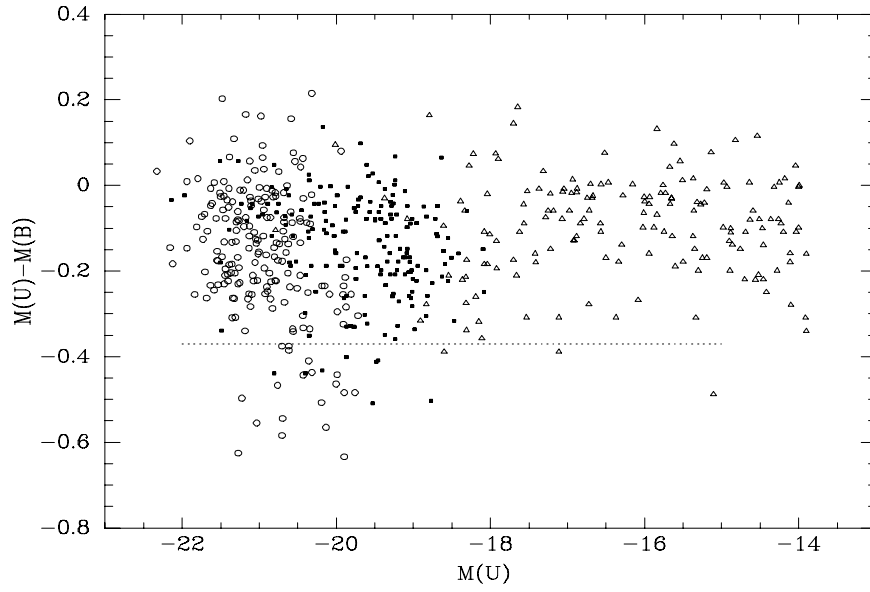


Fig. 8 Histograms of $(U-B)$ vs. galaxy number for the blue galaxy sample in three redshift bins and three absolute B magnitude bins. Each column contains galaxies in the same redshift bin, while each row contains galaxies in the same magnitude bin.

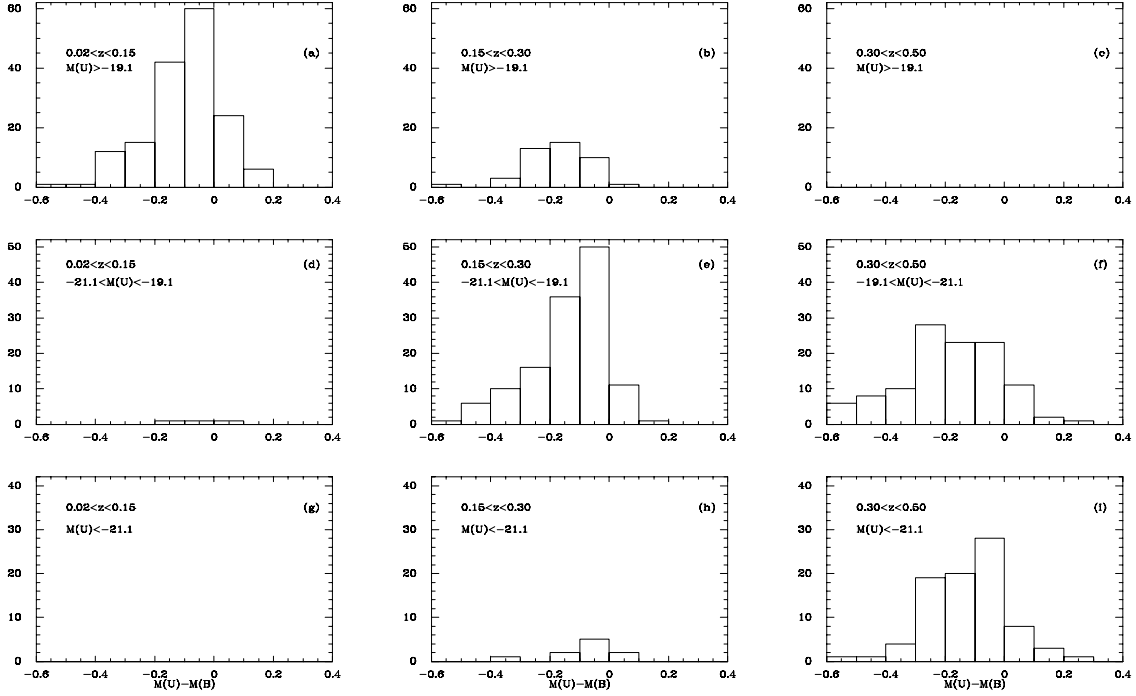


Fig. 9 Same as Figure 8, but with apparent magnitude limit reduced to $U \leq 20.8$ instead of 21.1.

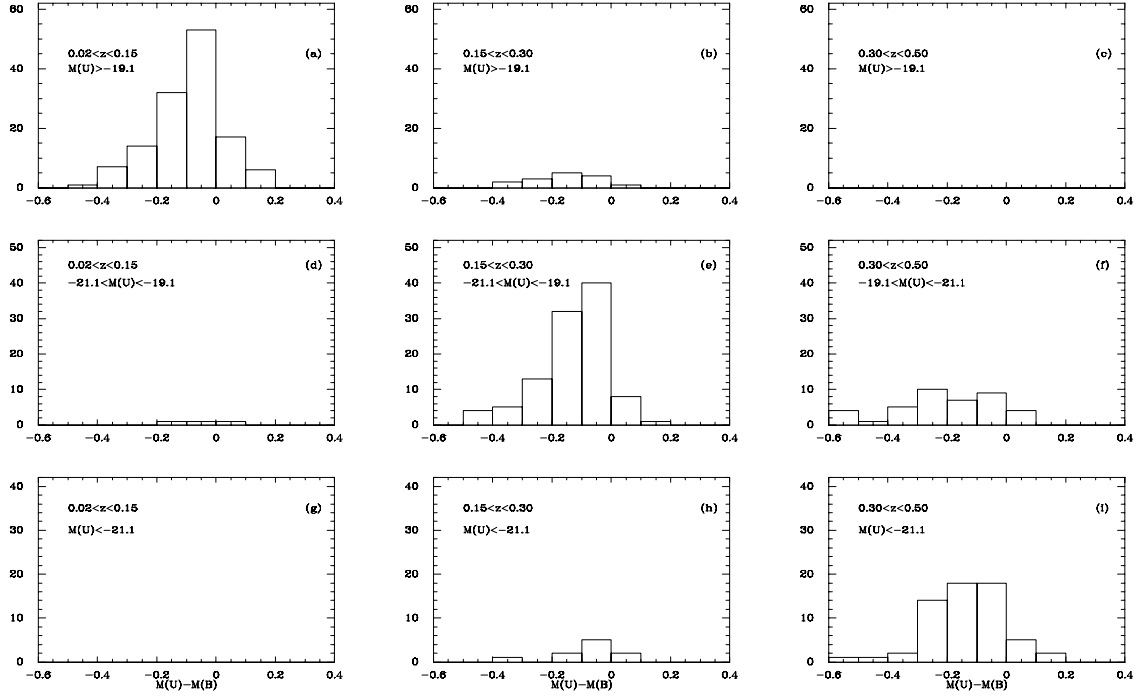


Fig. 10 Spectra of four of the excess blue galaxies. Photometric and spectroscopic redshifts for each galaxy are given. The spectral energy distribution of the Liu & Green (1998) starburst galaxy template (dotted lines), redshifted to each galaxy, is overplotted. Spectra are in units of F_λ ; wavelengths are in \AA .

